Soft Matter

FLIM-FRAPP: Near-Simultaneous Characterization of Multi-Scale Polymer Dynamics via Fluorescence Microscopy

Journal:	*Soft Matter*
Manuscript ID	SM-COM-03-2025-000260.R1
Article Type:	Communication
Date Submitted by the Author:	30-Apr-2025
Complete List of Authors:	Jutze, Mary Kate; University of Massachusetts Amherst, Polymer Science and Engineering Young, Walter; University of Massachusetts Amherst, Polymer Science and Engineering Combs, Jasney; Ball State University, Chemistry Drescher, Owen; University of Massachusetts Amherst, Physics Merchant, Siddh; University of Massachusetts Amherst, Polymer Science and Engineering Katsumata, Reika; University of Massachusetts Amherst, Polymer Science and Engineering

COMMUNICATION

FLIM-FRAPP: Near-Simultaneous Characterization of Multi-Scale Polymer Dynamics via Fluorescence Microscopy

Received 00th January 20xx,
Accepted 00th January 20xx

DOI: 10.1039/x0xx00000x

M. K. Jutze,[a] Walter W. Young, [a] Jasney M. Combs,[b] Owen C. Drescher,[c] Siddh Merchant,[d] and Reika Katsumata [*a]

Abstract

Characterizing multi-scale dynamics of polymers is crucial to inform property-process relationships, but there is an outstanding gap between accessibility and comprehensive data collection. To this end, we present a new multi-scale characterization method, FLIM-FRAPP, a near-simultaneous, hybrid approach between fluorescence lifetime measurement (FLIM) and fluorescence recovery after patterned photobleaching (FRAPP) to probe the glass transition temperature and self-diffusion coefficient of a model entangled copolymer, poly(methyl acrylate–stat–methyl methacrylate) (P(MA-stat-MMA)). Our investigation reveals opportunities and challenges concerning the nature of fluorescence characterization techniques for the exploration of polymer dynamics.

Chain dynamics across short and long length scales fundamentally inform a wide range of properties of polymeric materials both in solid and liquid states. The most well-studied short-range relaxation is segmental or α-relaxation, related to the glass transition temperature (T_g), at which the temperature dependence of the α-relaxation time changes drastically. Segmental relaxation dynamics and T_g dictate many solid-state properties, such as the dynamic modulus.[1] The self-diffusion coefficient (D) describes the other end of the dynamics length scale: entire-chain motion in a melt state. Self-diffusion is differentiated from other diffusion measurements by the lack of tracers involved; the only diffusion happening in the process is polymer diffusing through itself. T_g and D are related via the Williams-Landel-Ferry (WLF) equation,[2] and together inform the properties-processing-performance paradigm. Intimate knowledge of both solid- and melt-state properties of polymers, characterized by T_g and D, respectively, is crucial to guide optimal processing parameters for achieving ultimate performance.

Current common measurement methods for properties on different length scales often require separate samples and instruments. T_g can be measured by differential scanning calorimetry (DSC),[3] dynamic mechanical analysis (DMA),[1,4] dielectric spectroscopy,[5,6] and dilatometry.[4,7] D can be evaluated via small-angle neutron scattering (SANS),[8] elastic recoil detection (ERD),[9] secondary ion mass spectrometry (SIMS),[10,11] and forced Rayleigh scattering.[12] While informative, the above-mentioned methods require combining two techniques to obtain both T_g and D for a polymeric sample. Some require deuteration for labelling, an expensive and time-consuming modification. Neutron spin-echo (NSE) spectroscopy is excellent for characterizing the entire length-scale spectrum of dynamics, but often requires extremely long (multi-day) acquisition time and sample deuteration to obtain neutron contrast.[13] Another multi-scale characterization technique is electron spin resonance (ESR) spectroscopy, in which the temperature and relaxation time ranges are more limited compared to NSE.[14,15] Thus, there is an emerging need to bridge the gap between accessibility and comprehensive data collection.

To address this challenge, we propose a new hybrid method that combines fluorescence lifetime imaging microscopy (FLIM) and fluorescence recovery after patterned photobleaching (FRAPP), *FLIM-FRAPP,* as a time-efficient way of evaluating multi-scale polymer dynamics. **Figure 1a** is a schematic overview of FLIM-FRAPP. FRAPP is a well-accepted technique to measure D of polymers by monitoring fluorescence intensity changes of the bleached region over time.[16–19] In contrast to FRAPP, FLIM has been utilized for obtaining the T_g of limited polymeric systems,[20–22] although it is common as an imaging technique in life science.[23,24] Fluorescence lifetime ($\tau_{lifetime}$) is measured as the nanosecond-scale decay time between excitation of a fluorophore and detection of the corresponding emitted photon.[25] The $\tau_{lifetime}$ depends heavily on the sample environment, such as temperature or local rearrangement.[26,20,21] In particular, $\tau_{lifetime}$of fluorophores bonded to homopolymer

[a] University of Massachusetts Amherst, Department of Polymer Science and Engineering, 120 Governors Drive, Amherst MA 01003 USA
[b] Ball State University, Department of Chemistry, 622 N Martin Street, Muncie IN 47303 USA
[c] University of Massachusetts Amherst, Department of Physics, 710 North Pleasant Street, Amherst MA 01003 USA
[d] University of Massachusetts Amherst, Department of Chemical Engineering, 686 North Pleasant Street, Amherst MA 01003 USA
*Corresponding author: rkatsumata@umass.edu

Electronic Supplementary Information (ESI) available: Materials, labelled initiator synthesis, unlabelled and labelled copolymer synthesis, gel permeation chromatography, nuclear magnetic resonance spectroscopy, thermal gravimetric analysis, differential scanning calorimetry, self-quenching test, rheology, sample preparation, ellipsometry, FLIM-FRAPP details, Tg determination from FLIM, D determination from FRAPP, D determination from literature, and FRAPP Python script. See DOI: 10.1039/x0xx00000x

chains has been shown to decrease with increasing temperature at different linear rates above and below T_g.[20–22] Other methods of determining segmental dynamics from fluorescence phenomena do exist, including studies of rotational or temporal anisotropy of fluorescent probes[27–29] or of overall fluorescence intensity.[30–33] We have chosen to utilize FLIM over anisotropy or rotational measurements; the fluorophore we use must be small in size as to not hinder diffusion during FRAPP, and rotational dynamics only indirectly represent the interaction of the fluorophore with its local environment.[26] A similar and more well-studied way to measure T_g is by determining the kink temperature (temperature at which the slope changes) from fluorescence intensity versus temperature data. This approach leverages the temperature dependence of polymer segmental relaxation, which is highly related to fluorophore intensity.[34,35] It follows that a change in the local density would result in a change to the fluorophore's ability to transfer energy; it is not surprising that the slope changes during the glass transition. However, this established method is susceptible to artifacts arising from excitation laser intensity, sample geometry, and other sources.[34] Fluorescence lifetime, though a relatively new parameter in materials science, is a reliable and accurate monitor of atomic-scale rearrangements. However, the combination of FLIM with FRAPP has yet to be demonstrated. FLIM can be used nearly simultaneously with FRAPP because sample and instrumentation requirements are identical.

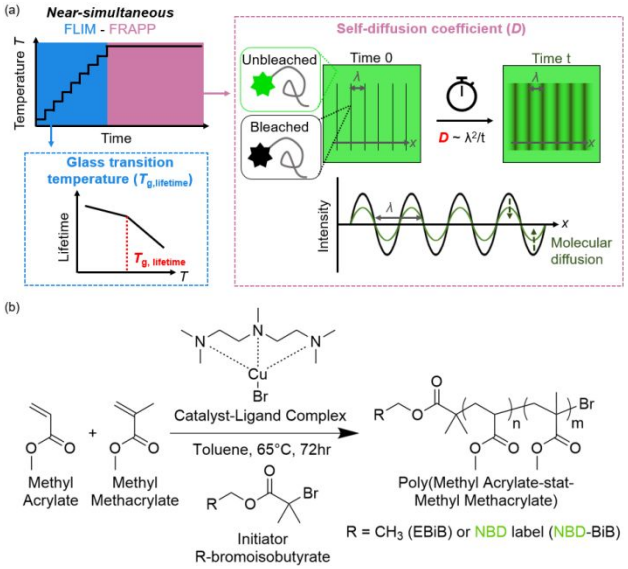

Figure 1. (**a**) Schematic illustration of near-simultaneous FLIM-FRAPP characterization. The temperature is increased stepwise over the course of a FLIM run and then held constant above T_g for the duration of the FRAPP measurement. (**b**) Reaction scheme for random copolymerization of methyl acrylate and methyl methacrylate via ATRP.

The use of fluorophores as probes for polymer dynamics is what allows such a combination of different measurements. Fluorophores can be covalently bonded anywhere in a polymer chain without significant effect on short- or long-range dynamics,[17,32,36,37] providing a degree of certainty that actual polymer dynamics are being measured as opposed to tracer dynamics. Their use circumvents the need for deuteration, long experiment runtimes, and expensive equipment usage. In our study, nitrobenzofurazan (nitrobenzoxadiazole or NBD) specifically has been chosen as a model fluorophore due to its relatively small size, ease of addition to the initiator via the chlorine leaving group from commercially available NBD-Cl, and pre-established capability for both FLIM[22] and FRAPP.[17,19] Statistical copolymer poly(methyl acrylate-stat-methyl methacrylate) (P(MA-stat-MMA)) is chosen as a model system due to the amorphous nature of atactic, low molecular weight acrylate polymers (eliminating potential artifacts from crystallization) and because of the ease with which T_g can be tailored to match the biologically-relevant temperature range (~5-55 °C) in our equipment by changing the monomer feed ratio. This work reports the capability of FLIM-FRAPP, which enables near-simultaneous measurement of T_g and D within several hours.

P(MA-stat-MMA) was synthesized via atom-transfer radical polymerization (ATRP) using either ethyl-α-bromoisobutyrate as initiator for unlabelled polymer or NBD-functionalized initiator[17] (NBD-bromoisobutyrate or NBD-BiB, **Scheme S1**) for NBD-labelled polymer (**Figure 1b)**. Chemical structure and comonomer ratios were verified by ^{1}H nuclear magnetic resonance (NMR) spectroscopy (**Figure S1**) and molecular weight by gel permeation chromatography (GPC) (**Figure S2**, **Table 1**). All polymer samples were completely dried under vacuum prior to thermal evaluation by thermal gravimetric analysis (TGA) (**Figure S3**) and DSC (**Figure S4**, **Table 1**). To avoid self-quenching, 10 wt% of labelled copolymer was mixed with 90 wt% of unlabelled copolymer, which is well below the self-quenching limit at which the linear relationship between intensity and concentration breaks down (**Figure S6**). The final comonomer ratio of the labelled and unlabelled blend was calculated (by ^{1}H NMR) to be 57 mol% MA to 43 mol% MMA (average of the two components). Films were prepared by spin coating from toluene onto UV-Ozone treated glass slides, and then dried and annealed overnight in a vacuum furnace (<1 mTorr) at 60°C. Their thickness was measured via ellipsometry to be between 165-170 nm. Detailed synthesis and sample preparation procedures can be found in the Supplementary Information. FLIM and FRAPP measurements were conducted on a Nikon Eclipse Ti A1 scanning confocal laser microscope equipped with a Tokai Hit TP-CHSQ-C temperature-controlled stage. During a FLIM run, the films were alternately heated at a rate of ~0.7 °C/min and held at temperature, during which lifetime was measured. Once the full temperature sweep was complete, the films were above measured T_g of the labelled-unlabelled copolymer blend (31.2 ± 2 °C by DSC), providing ideal conditions for FRAPP measurement at 53 °C. Full FLIM-FRAPP characterization for one film is completed in a few hours.

Table 1. Molecular weight, dispersity, and glass transition temperature measured by DSC for both copolymers.

	M_n, kDa	Đ	T_g, °C
P(MA_{58}-stat-MMA_{42})	28.4	1.19	37.1 ± 2
NBD-P(MA_{52}-stat-MMA_{48})	36.8	1.20	53.5 ± 2

The D values measured by FRAPP display good repeatability across samples. **Figure 2a** shows a representative fluorescence

microscopy image at the initial (t = 0 min) time at 53 °C with a bleached pattern with a wavelength (λ) of 18.64 ± 0.04 μm, where the baseline was corrected using both a pre-bleach background as well as a baseline intensity normalization for each time scan shown as a solid box in **Figure 2a**. The y-averaged intensity of the region of interest (ROI, shown as a dashed box in **Figure 2a**) is plotted against x-distance, resulting in a sinusoidal profile in **Figure 2b**. The time decay of the amplitude $A(t)$ of this profile (peak minima subtracted from peak maxima) divided by the initial amplitude, $A(t = 0$ min) or A_0 is shown in **Figure 2c**. D corresponds to the slope of this relationship because the decay of $A(t)/A_0$ originates from NBD-labelled polymers diffusing into and out of the bleached or unbleached regions. In other words, D is calculated by **Equation 1**:

$$\ln\left(A(t)\,/A_0\right) = -4\pi^2 Dt/\lambda^2 = mt \qquad \textbf{Equation 1}$$

where the slope $m = -4\pi^2 D/\lambda^2$ (see SI for details). A Python script (**SI, Appendix**) was used to process FRAPP data to calculate D as detailed in the Supporting Information.

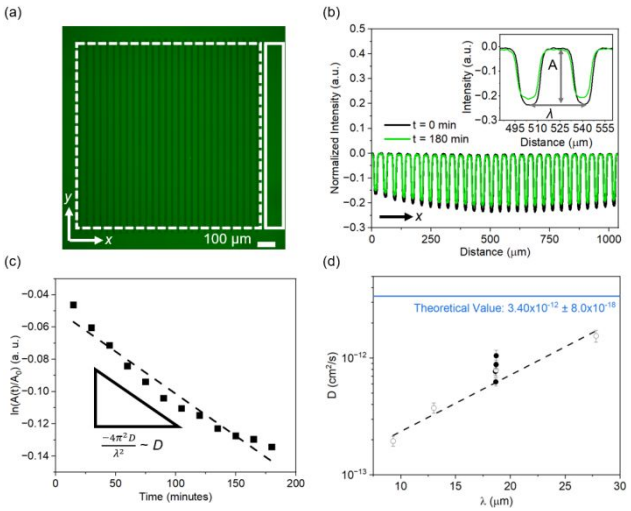

Figure 2. (**a**) Example fluorescence image taken at t = 0 for one FRAPP run. The dashed box represents the ROI and the solid box the background region. The scale bar represents 100 μm. (**b**) Plot of normalized fluorescence intensity over distance for both the example image t = 0 and the final scan at t = 180 minutes. The inset shows A, the amplitude, and λ, the wavelength of the sinusoid profile. (**c**) Fluorescence intensity for each scan normalized by A_0 and plotted against time. The slope of the linear relationship corresponds to D. (**d**) D of P(MA-stat-MMA) obtained via FRAPP for two different experimental setups compared to the value estimated from experimentally measured zero-shear viscosity and literature values of density, end-to-end distance, and entanglement molecular weight.[51,52] Error bars represent propagated standard error.

The experimental D values (**Figure 2d**) are compared to two validation methods. First, the diffusion coefficient is plotted against varying tested wavelengths (open circles in **Figure 2d**). In theory, D should not depend on λ to such a degree (R^2 = 0.932); a polymer chain beginning its journey inside a wider bleached region should take a longer time to pull the bleached fluorophore into an unbleached region (and vice versa) than one inside a smaller region. Previous work has shown similar issues with arbitrarily choosing an observation area around a Gaussian spot bleach;[38] the final D value scales with the size of the area around the bleached spot that is observed, but is still independent of the spot size. While there is little investigation into the effect of a bleached pattern upon the calculated D in polymeric systems, analysis via Fourier transform may resolve this issue in the future.[39]

Second, a value for D was calculated with the reptation model ($3.4\times10^{-12} \pm 8.0\times10^{-18}$ cm^2/s),[8,40–42] because the molecular weights of the polymers used in this study were higher than the critical entanglement molecular weight (M_c) for both PMA (~10 kDa) and PMMA (~6.7 kDa),[43,44] i.e. our system is entangled. The theoretical value was estimated with Graessley's equation[41] based on Doi-Edwards theory for the reptation model[40] as detailed in the SI:

$$D = (kT\rho N_A R_g^2)/(6\eta_0 M_e) \qquad \textbf{Equation 2}$$

where k is the Boltzmann constant, T is the temperature, ρ is the density, N_A is Avogadro's number, R_g^2 is the mean-squared radius of gyration of the polymer, η_0 is the zero-shear viscosity, and M_e is the molecular weight between entanglements. The values of $\langle r^2\rangle/M$ (used to calculate R_g^2), M_e (equal to one half M_c), and ρ for homopolymer PMA and PMMA were obtained from literature and averaged based on monomer composition to calculate D.[43,44] This averaging method may not fully represent the dynamically asymmetric copolymer blend; however, there is no data available in the literature for better estimation of such a system. The zero-shear viscosity of the blend at 53 °C was obtained via small-amplitude oscillatory rheology (**Figure S5**). There is a difference between experimentally observed D values and the predicted value. Any potential temperature difference between rheology and FRAPP, even at opposite bounds of the error in temperature measurement, would not decrease the theoretical calculation's order of magnitude. It is our belief that the discrepancy arises from the timescale on which FRAPP measurements were performed; due to the equipment's limitation on temperature, the bleached region does not see a significant return to a pre-bleached state, as can be seen in other FRAP/FRAPP studies of faster systems.[45] To avoid a dependence on the bleached pattern size and while limited to our current equipment, future work may investigate lower T_g materials such that faster dynamics and full bleaching recovery can be observed.

FLIM measurements revealed that $\tau_{lifetime}$ of fluorophores attached to the polymer decreased with increasing temperature (T), with a slope change near T_g. **Figure 3a** shows examples of $\tau_{lifetime}$ maps at the lowest (7.6 °C) and the highest (55.2 °C) temperatures during a run for one of the samples; the lifetime for each temperature was calculated as the average over the observed ~0.4 mm^2 area, yielding $\tau_{lifetime}(T)$. As shown in **Figure 3b**, $\tau_{lifetime}$ decreased as temperature increased with a slope change near $T_{g,DSC}$, consistent with previous studies.[20–22] The kink temperature ($T_{g,lifetime}$) is determined as 38.4 ± 3.0 °C by fitting to a hyperbolic cosine function, as used by Dalnoki-Veress et al.[46] for thickness-temperature measurements (**Equation S2**). This equation is empirical; it is intended to mathematically identify the slope transition between two linear

regions in a dataset without bias. The shaded temperature range shown reflects standard error from the fitting process. Five runs were performed in total; the average $T_{g,lifetime}$ for the samples was 36.0 ± 2.8 °C (1 standard deviation). To assess this kink temperature from FLIM measurements, the T_g of both labelled and unlabelled copolymers used, in addition to that of the blended system, were measured by DSC ($T_{g,DSC}$) at a heating rate of 0.7 °C/min (**Figure S4**, **Table 1**).

Previous observations showed a closer match between $T_{g,DSC}$ and $T_{g,lifetime}$ for a PS-NBD system compared to our FLIM results for NBD-P(MA-stat-MMA).[20–22] Curiously, T_g as estimated by the Fox equation:[47]

$$1/T_g = w_1/T_{g1} + w_2/T_{g2} \quad \textbf{Equation 3}$$

$T_{g,Fox}$ = 311.7 K (38.7 °C) matches $T_{g,lifetime}$ closely, while $T_{g,DSC}$ of the blend is much lower. There is only a small difference in heating rate between DSC and FLIM; all measurements took place at ~0.7 °C/min. There should not be significant confinement effects in the FLIM measurements, as all thin film samples are above 100 nm thick, allowing them to be considered as bulk.[21] Additionally, previous study of the relationship between fluorophore tether location and observed dynamics has not found meaningful differences between mid- and end-chain dynamics, indicating our measurements are likely not sensitive to the fluorophore's position at the end of the polymer chains.[17,36]

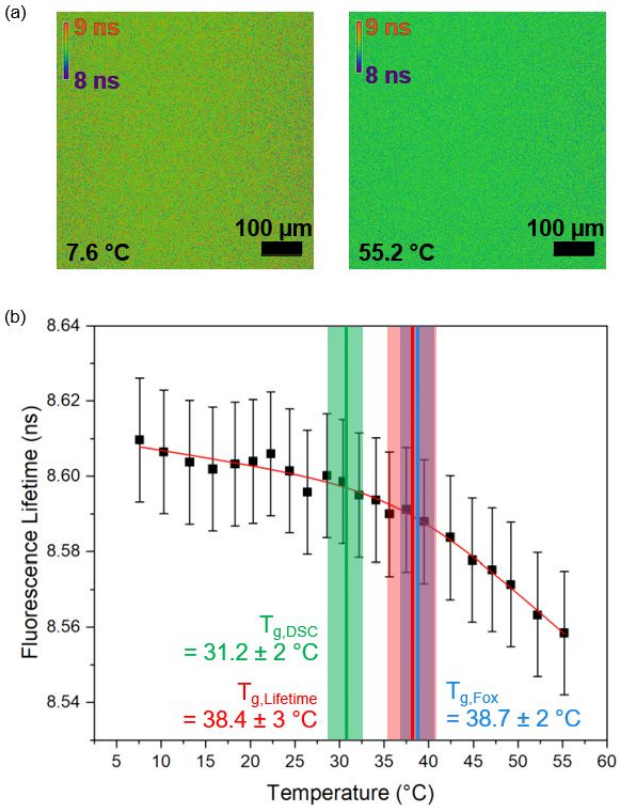

Figure 3. (**a**) Colour maps of fluorescence lifetime in a representative NBD-P(MA-stat-MMA) thin film taken at 7.6 °C (left) and 55.2 °C (right) and displaying average fluorescence lifetimes of 8.61 ± 0.02 ns and 8.56 ± 0.02 ns, respectively. The color-coding scale on the left is from 8 (violet) to 9 ns (red), and the scale bars represent 100 µm. (**b**) Corresponding full plot of fluorescence lifetime versus temperature. Error bars represent a 95% confidence interval. The vertical lines indicate $T_{g,DSC}$, $T_{g,Fox}$, and $T_{g,lifetime}$. The curve is fit with a hyperbolic cosine function.[46]

We hypothesize that the difference of T_g from DSC and FLIM comes from the dynamically asymmetric nature of a P(MA-stat-MMA) copolymer. Homopolymers of PMA and PMMA exhibit ~ 110 °C difference in T_g ($T_{g,PMA}$ = –1 °C, $T_{g,PMMA}$ = 112 °C),[14,48] which means our statistical copolymer could have significant dynamic heterogeneity. While PMA and PMMA are immisible,[49] we do not expect significant phase separation in the blend because there is no secondary T_g seen from DSC (**Figure S4**).

T_g as calculated by the Fox equation represents ideal, random mixing. T_g of the blend system as measured by DSC is lower than that predicted by random mixing (or by FLIM, which reports an average of many localized density fluctuations). This would suggest DSC is more sensitive to the mobile component in the blend, while the average of many local lifetime measurements is closer to an approximation of random mixing. Interestingly, Mbonu et al. reported that T_g of a dPMMA/hPMA blend measured by Fixed Window Scans (FWS) in quasi-elastic neutron scattering (QENS) was ~ 7 °C higher than T_g measured by DSC, but identical for hPMA and hPMA/dPS blend.[49] QENS measures mean-square displacement, which is more proxy to fluorescent lifetime. These characterization methods, while able to monitor very local behaviour, may lose sight of the dynamic heterogeneity in the system (i.e., mobile MA and immobile MMA segments) due to the averaging of data.

In summary, we report the combination of fluorescence lifetime measurement and fluorescence recovery after patterned photobleaching, or FLIM-FRAPP, to address the challenge in accessibility in conventional polymer dynamics measurement. Sequential characterization of FLIM and FRAPP was completed within a few hours. FRAPP measurement shows an unexpected dependence on pitch size, which prompts further investigation. The method is best used as a comparison between samples with the same bleached pattern. In addition, both FLIM and FRAPP's unique mapping capabilities, as well as FLIM's use as a local dynamics detection method, are well-suited for monitoring heterogeneous systems or multiple properties beyond T_g.[50–53] We hope to further demonstrate the capabilities of fluorescence measurement outside of the glass transition in future work.

Author Contributions

The manuscript was written through contributions of all authors. RK was responsible for investigation conceptualization, acquisition of resources and funding, and project supervision. MKJ was responsible for writing the original draft. MKJ and JC were responsible for visualization. RK, WY, and MKJ were responsible for project administration and developing a methodology. MKJ, WY, JC, OD, and SM were responsible for data curation and analysis. All authors contributed to investigation, validation, and writing review and editing. All authors have given approval to the final version of the manuscript.

Data Availability

The data supporting this manuscript, including code used for FRAPP analysis, are included in the Supplementary Information.

Acknowledgements

RK thanks NSF CAREER Award DMR # 2046606, 3M Non-Tenure Faculty Award, and UMass Amherst Startup Funding. The authors deeply appreciate the University of Massachusetts Institute for Applied Life Sciences Light Microscopy Facility and the associated expertise and insight of Dr. James Chambers, Dr. Maaya Ikeda, and Dimitri Nikolla. The authors gratefully recognize the aid of Shiqi Liu at the University of Massachusetts Amherst for collection of the zero-shear viscosity data. JC thanks the University of Massachusetts Advancing Science and Engineering for Diverse Scholars (ASCENDS) Program. MKJ thanks Stephen J. Rosa at Agilent Technologies, and the Kandula Research Group as well as Dr. Autumn M. Mineo, Dr. Roshni J. Chethalen, Dr. Shota Fujii, Elizabeth Haljun, and Tomoko Yamazaki at the University of Massachusetts Amherst, for their expertise and insightful discussions.

Conflicts of interest

There are no conflicts to declare.

References

1 Y. Wada, H. Hirose, T. Asano and S. Fukutomi, *J. Phys. Soc. Jpn.*, 1959, **14**, 1064–1072.
2 M. L. Williams, R. F. Landel and J. D. Ferry, *J. Am. Chem. Soc.*, 1955, **77**, 3701–3707.
3 A. J. Müller and R. M. Michell, in *Polymer Morphology*, John Wiley & Sons, Ltd, 2016, pp. 72–99.
4 G. Rotter and H. Ishida, *Macromolecules*, 1992, **25**, 2170–2176.
5 G. Williams, *Trans. Faraday Soc.*, 1964, **60**, 1556–1573.
6 I. Popov, S. Cheng and A. P. Sokolov, in *Macromolecular Engineering*, John Wiley & Sons, Ltd, 2022, pp. 1–39.
7 S. Saito and T. Nakajima, *J. Appl. Polym. Sci.*, 1959, **2**, 93–99.
8 C. R. Bartels, B. Crist and W. W. Graessley, *Macromolecules*, 1984, **17**, 2702–2708.
9 R. J. Composto, R. M. Walters and J. Genzer, *Mater. Sci. Eng. R Rep.*, 2002, **38**, 107–180.
10 S. A. Schwarz, B. J. Wilkens, M. A. A. Pudensi, M. H. Rafailovich, J. Sokolov, X. Zhao, W. Zhao, X. Zheng, T. P. Russell and R. A. L. Jones, *Mol. Phys.*, 1992, **76**, 937–950.
11 H. Yokoyama, E. J. Kramer, M. H. Rafailovich, J. Sokolov and S. A. Schwarz, *Macromolecules*, 1998, **31**, 8826–8830.
12 M. Wang, K. Timachova and B. D. Olsen, *Macromolecules*, 2015, **48**, 3121–3129.
13 D. Richter, R. Butera, L. J. Fetters, J. S. Huang, B. Farago and B. Ewen, *Macromolecules*, 1992, **25**, 6156–6164.
14 L. Andreozzi, C. Autiero, M. Faetti, M. Giordano and F. Zulli, *J. Non-Cryst. Solids*, 2006, **352**, 5050–5054.
15 Y. Miwa and K. Yamamoto, *J. Phys. Chem. B*, 2012, **116**, 9277–9284.
16 B. Frank, A. P. Gast, T. P. Russell, H. R. Brown and C. Hawker, *Macromolecules*, 1996, **29**, 6531–6534.
17 J. M. Katzenstein, D. W. Janes, H. E. Hocker, J. K. Chandler and C. J. Ellison, *Macromolecules*, 2012, **45**, 1544–1552.
18 K. Geng, R. Katsumata, X. Yu, H. Ha, A. R. Dulaney, C. J. Ellison and O. K. C. Tsui, *Macromolecules*, 2017, **50**, 609–617.
19 R. Katsumata, A. R. Dulaney, C. B. Kim and C. J. Ellison, *Macromolecules*, 2018, **51**, 7509–7517.
20 K. Tanaka, Y. Tsuchimura, K. Akabori, F. Ito and T. Nagamura, *Appl. Phys. Lett.*, 2006, **89**, 061916.
21 K. Tanaka, Y. Tateishi, Y. Okada, T. Nagamura, M. Doi and H. Morita, *J. Phys. Chem. B*, 2009, **113**, 4571–4577.
22 D. Kawaguchi, Y. Tateishi and K. Tanaka, *J. Non-Cryst. Solids*, 2015, **407**, 284–287.
23 P. Keshri, B. Zhao, T. Xie, Y. Bagheri, J. Chambers, Y. Sun and M. You, *Angew. Chem. Int. Ed.*, 2021, **60**, 15548–15555.
24 R. Datta, T. M. Heaster, J. T. Sharick, A. A. Gillette and M. C. Skala, *J. Biomed. Opt.*, 2020, **25**, 071203.
25 J. Lakowicz, *Principles of Fluorescence Spectroscopy*, 3rd edn., 2006.
26 G. Hinze, T. Basché and R. a. L. Vallée, *Phys. Chem. Chem. Phys.*, 2011, **13**, 1813–1818.
27 P. D. Hyde, M. D. Ediger, T. Kitano and K. Ito, *Macromolecules*, 1989, **22**, 2253–2259.
28 A. Dhinojwala, J. C. Hooker and J. M. Torkelson, *J. Non-Cryst. Solids*, 1994, **172–174**, 286–296.
29 S. Lee, J. Choi, J. Choe, M. Kim and K. Paeng, *J. Chem. Phys.*, 2018, **149**, 164910.
30 C. J. Ellison, R. L. Ruszkowski, N. J. Fredin and J. M. Torkelson, *Phys. Rev. Lett.*, 2004, **92**, 095702.
31 R. D. Priestley, M. K. Mundra, N. J. Barnett, L. J. Broadbelt, J. M. Torkelson, R. D. Priestley, M. K. Mundra, N. J. Barnett, L. J. Broadbelt and J. M. Torkelson, *Aust. J. Chem.*, 2007, **60**, 765–771.
32 D. Christie, R. A. Register and R. D. Priestley, *ACS Cent. Sci.*, 2018, **4**, 504–511.
33 Y. Han and C. B. Roth, *Soft Matter*, 2022, **18**, 6094–6104.
34 M. K. Mundra, C. J. Ellison, P. Rittigstein and J. M. Torkelson, *Eur. Phys. J. Spec. Top.*, 2007, **141**, 143–151.
35 C. J. Ellison and J. M. Torkelson, *J. Polym. Sci. Part B Polym. Phys.*, 2002, **40**, 2745–2758.
36 J. Choi, S. Lee, J. Choe, Y. Chung, Y. E. Lee, J. Kim, M. Kim and K. Paeng, *ACS Macro Lett.*, 2019, **8**, 1181–1186.
37 H. Lee, D. Son, S. Lee, K. Eun, M. Kim and K. Paeng, *Macromolecules*, 2022, **55**, 8176–8185.
38 D. Blumenthal, L. Goldstien, M. Edidin and L. A. Gheber, *Sci. Rep.*, 2015, **5**, 11655.
39 A. C. Geiger, C. J. Smith, N. Takanti, D. M. Harmon, M. S. Carlsen and G. J. Simpson, *Biophys. J.*, 2020, **119**, 737–748.
40 M. Doi and S. F. Edwards, *J Chem Soc Faraday Trans 2*, 1978, **74**, 1802–1817.
41 W. W. Graessley, *J. Polym. Sci. Polym. Phys. Ed.*, 1980, **18**, 27–34.
42 D. S. Pearson, G. Ver Strate, E. Von Meerwall and F. C. Schilling, *Macromolecules*, 1987, **20**, 1133–1141.
43 S. Wu, *J. Polym. Sci. Part B Polym. Phys.*, 1989, **27**, 723–741.
44 L. J. Fetters, D. J. Lohse and W. W. Graessley, *J. Polym. Sci. Part B Polym. Phys.*, 1999, **37**, 1023–1033.
45 N. Lorén, J. Hagman, J. K. Jonasson, H. Deschout, D. Bernin, F. Cella-Zanacchi, A. Diaspro, J. G. McNally, M. Ameloot, N. Smisdom, M. Nydén, A.-M. Hermansson, M. Rudemo and K. Braeckmans, *Q. Rev. Biophys.*, 2015, **48**, 323–387.
46 K. Dalnoki-Veress, J. A. Forrest, C. Murray, C. Gigault and J. R. Dutcher, *Phys. Rev. E*, 2001, **63**, 031801.
47 T. G. Fox, *Bull. Am. Phys. Soc.*, 1956, **1**, 123.
48 B. Lu, K. Lamnawar, A. Maazouz and H. Zhang, *Soft Matter*, 2016, **12**, 3252–3264.
49 C. Mbonu, N. C. Osti, D. Wu and P. Akcora, *J. Polym. Sci.*, 2024, **62**, 4177–4185.
50 Z. Cao, D. M. Harmon, R. Yang, A. Razumtcev, M. Li, M. S. Carlsen, A. C. Geiger, D. Zemlyanov, A. M. Sherman, N. Takanti,

J. Rong, Y. Hwang, L. S. Taylor and G. J. Simpson, *Anal. Chem.*, 2023, **95**, 2192–2202.
51 H. Vu, J. W. Woodcock, A. Krishnamurthy, J. Obrzut, J. W. Gilman and E. B. Coughlin, *ACS Appl. Mater. Interfaces*, 2022, **14**, 10793–10804.
52 T. Shiga, A. Okada, H. Takahashi and T. Kurauchi, *J. Mater. Sci. Lett.*, 1995, **14**, 1754–1756.
53 H. Liu, Z. Hu, Q. Li and X. Ji, *Macromolecules*, 2023, **56**, 8003–8010.

Data Availability

The data supporting this manuscript, including code used for FRAPP analysis, are included in the Supplementary Information.